

# Temporal structure of human magnetic evoked fields

David P. Crewther<sup>1</sup> · Alyse Brown<sup>1</sup> · Laila Hugrass<sup>1</sup>

Received: 15 December 2015 / Accepted: 16 February 2016 / Published online: 7 March 2016  
© Springer-Verlag Berlin Heidelberg 2016

**Abstract** Nonlinear analysis of the multifocal cortical visual evoked potential has allowed the identification of neural generation of higher-order nonlinear components by magnocellular and parvocellular neural streams. However, the location of individual brain sources that make such contributions to these evoked responses has not been studied. Thus, an *m*-sequence pseudorandom stimulus system was developed for use in magnetoencephalographic (MEG) studies. Five normal young adults were recorded using an Elekta TRIUX MEG with 306 sensors. Visual stimuli comprised a nine-patch dartboard stimulus, and each patch fluctuated between two luminance levels with separate recordings carried out at low (24 %) and high (96 %) temporal contrast. Sensor-space analysis of MEG evoked fields identified components of the first- and second-order Wiener kernel decomposition that showed qualitative similarity with EEG-based cortical VEP recordings. The first slice of the second-order response (K2.1) was already saturated at 24 % contrast, while the major waveform of the second slice of the second-order response (K2.2) grew strongly with contrast, consistent with properties of the magnocellular and parvocellular neurons. Minimum norm estimates of cortical source localization showed almost simultaneous activation of V1 and MT+ activations with latencies only a little greater than those reported for first neural spikes in primate single cell studies. Time–frequency analysis of the kernel responses from five minimum norm estimate scout sources shows contributions from higher-frequency bands

for the first compared with the second slice response, consistent with the proposed neural sources. In support of this magno/parvo break-up, the onset latencies of the K2.2 responses were delayed by approximately 30 ms compared with K2.1 responses.

**Keywords** Magnocellular · Parvocellular · MEG · Nonlinearity · Latency · MT+

## Introduction

Across the primate species, the lateral geniculate nucleus (LGN) is characterized by two ventral M-magnocellular layers of large cells and a series (four in human) of smaller cell P-parvocellular layers located more dorsally. In addition, there is a less laminated distribution of koniocellular neurons with tiny cell somata. Primate neurophysiologists (Kaplan and Shapley 1986; Maunsell et al. 1999) have established that geniculate M neurons demonstrate relatively high contrast gain, response saturation at high contrast, low chromatic sensitivity and high temporal frequency cut-offs compared with the P neurons, which typically show chromatic tuning, high spatial sensitivity, lower contrast gain without saturation, and lesser temporal frequency performance.

Cortically, however, the separation of magnocellular and parvocellular contributions becomes more complicated (Nassi and Callaway 2009), with mixing of M and P inputs at early cortical levels. Despite this, two basic streams of visual processing have been identified—the vision for perception set of visual cortical areas extending from occipital cortex into the temporal lobe, and the vision for action dorsal cortical stream comprising multiple representations in parietal cortex.

✉ David P. Crewther  
dcrewther@swin.edu.au

<sup>1</sup> Centre for Human Psychopharmacology, Swinburne University of Technology, 1 Alfred St, Hawthorn, Melbourne 3122, Australia

The development of multifocal ERG techniques through the VERIS system (EDI, San Mateo, USA) (Sutter 1992) provided multiple decorrelated pseudorandom binary stimuli to test retinal responses across the visual field. The random stimulation also allows for the analysis of higher-order kernels through the Wiener kernel decomposition (Sutter 1992). These techniques for multifocal visual field mapping have been extended from retina to cortex (Baseler et al. 1994), with immediate application for using cortical visual evoked potentials to monitor retinal disease (Hood and Greenstein 2003) and then to MRI and MEG techniques. Multifocal fMRI mapping (Henriksson et al. 2012; Vanni et al. 2005) provides complementary information to the more conventional phase encoding methods (Engel et al. 1994; Sereno et al. 1995). Multifocal MEG has been employed for establishing retinotopy, mainly with contrasting reversing stimuli and analysed usually with dipole fitting methods (Nishiyama et al. 2004; Tabuchi et al. 2002).

A breakthrough in the biological significance of higher-order kernels came with the realization that slices of the second-order kernels mimicked the contrast response and saturation of LGN magnocellular and parvocellular neurons (Klistorner et al. 1997). These kernel slices largely separated the M and P contributions as a function of interaction time. In addition, there was a 25-ms latency difference between peaks of cortical activation observed for these waveforms, giving priority to magnocellularly driven information in cortical processing. Such latency advantage—termed the magnocellular advantage (Laycock et al. 2007, 2008)—supports the notion that early information reaching primary visual cortex has sufficient time to feed forward to early dorsal cortical areas and back to V1 to coordinate with parvocellular input (Bullier 2001). The role of such retro-injection appears to lie in figure/ground segmentation (Hupe et al. 1998, 2001; Super and Lamme 2007a, b).

The current research extends the study of temporal nonlinearities in visual evoked response from VEP to MEG, particularly investigating the timing of activation of visual cortex by the magnocellular and parvocellular streams, and importantly, allowing estimation of order of activation of such brain sources, testing the hypotheses inherent in the notion of the magnocellular advantage (Laycock et al. 2007). VEP typically is recorded from a single electrode over occipital cortex. As such, it is insensitive to the location of multiple brain sources of signal. MEG using several hundred sensors is better able to localize sources than EEG mainly because of the transparency of the skull to magnetic fields. Thus, our intention was to study the temporal (non-linear) structure of the visual evoked magnetic fields with an aim of locating brain sources and measuring the relative timing of their activations.

## Methods

### Participants

Upon approval from the Swinburne Human Research Ethics Committee, five young adult participants were recruited for the MEG study and gave written informed consent (in accordance with the Declaration of Helsinki) prior to testing. They had normal or corrected-to-normal vision.

### Stimuli

A set of pseudorandom  $m$ -sequence binary temporal codes was programmed using LabView (National Instruments, USA). A 9-segment dartboard stimulus (circular centre patch with two rings of 4 segments) was programmed in VPixx (<http://www.VPixx.com>—see Fig. 1a). Each segment was diffusely coloured and fluctuated between two luminance levels using the  $m$ -sequence ( $m = 14$ ) broken into 4 segments of approximately 1 min. The sequences were maximally offset in time so that mutual decorrelation was achieved, allowing the independent simultaneous recording from each patch. Only the central patch, subtending  $4^\circ$  of visual angle, when viewed at 120 cm, was analysed in the current paper, as our primary interest was to extend the study of higher-order Wiener kernels from EEG-based visual evoked potentials to MEG recordings. Two separate acquisitions were made with binary stimulation between black and white (96 % temporal contrast) and two levels of grey (24 % contrast). The stimuli were projected into the magnetically shielded room via a data projector operating at a frame rate of 60 Hz. Triggers were set and reset for stimulus onset and offset, respectively, allowing for first order and the first two slices of the second-order kernels to be easily estimated. The participants had no task to perform apart from keeping fixation on the centre of the stimulus.

### MEG

MEG recordings were made using an Elekta TRIUX MEG scanner with 102 magnetometer and 204 planar gradiometer SQUID detectors. Recordings were carried out in a dimly illuminated magnetically shielded (two layers of  $\mu$ -metal and one layer of copper) room (MSR) with active shielding coils within and outside the MSR in order to provide active shielding of magnetic transients. Only the first- and second-order responses from the central patch were analysed.

Each 4-min recording resulted in  $2^{14}-1$  frames of stimulation. The VPixx binary stimulus sent different triggers to the MEG recording system each time stimulus level 1

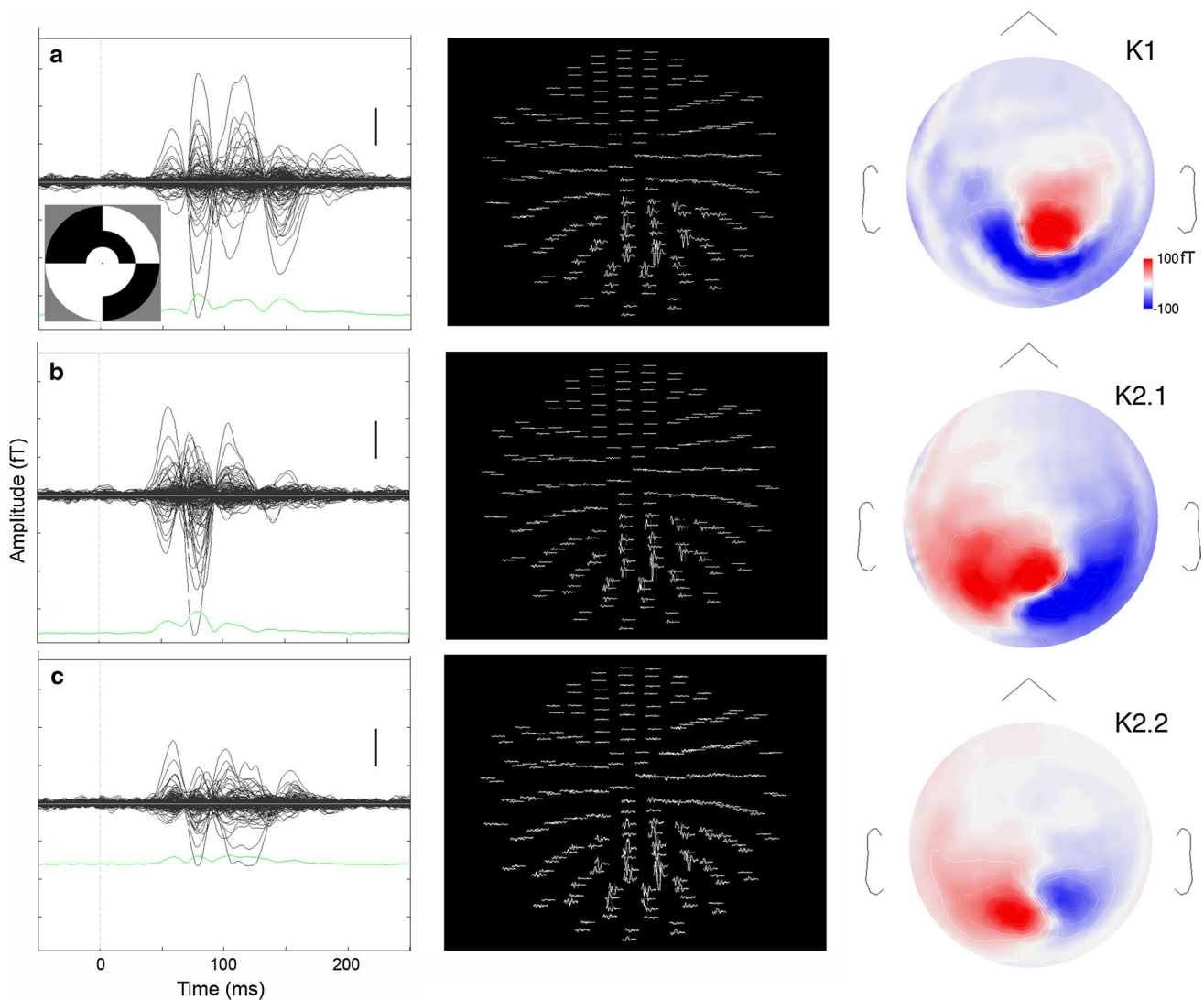


**Fig. 1** Butterfly plots, sensor array maps and interpolated sensor amplitudes (from the planar gradiometers) for participant R1054. The first-order response K1 is shown in (a) along with the 96 % contrast multifocal stimulus (shown as an *inset*). The first two slices of the second-order kernel K2.1, K2.2 are shown in (b, c). Note that these kernel elements K1, K2.1 and K2.2 are derived from the same recordings. The recordings show good signal-to-noise ratio, with a concentration of response centred over occipital sensors. Compar-

ing Fig. 1a–c, both the butterfly plots and the interpolated disc plots show differences in timing and in relative strength of the peaks. In particular, the response density shown at the latency (79 ms) in the disc plots shows evident difference between K1 and K2.1 in terms of a best fitting dipole for such a field distribution. *Scale bars* (butterfly plots) represent 100fT. In a–c, the *green line* represents the global field potential, and the *scale bar* represents 100fT

or stimulus level 2 was set. The first-order kernel (K1) is the sum of all responses to stimulus one ( $R_1$ ) minus the sum of all responses to stimulus two ( $R_2$ ) throughout the perfectly balanced pseudorandom sequence, i.e.  $0.5 \cdot (R_1 - R_2)$  (Sutter 1992). The first two slices of the second-order response (K2.1 and K2.2) of the MEG evoked fields (MEF) were similarly extracted (Klistorner et al. 1997; Sutherland and Crewther 2010). The second-order response takes account of the history of stimulation, with the first slice (K2.1) representing a comparison between two consecutive frames when a transition

has occurred ( $R_{12}, R_{21}$ ) and where a transition has not occurred ( $R_{11}, R_{22}$ ), i.e.  $K2.1 = 0.25 \cdot (R_{11} + R_{22} - R_{12} - R_{21})$ . The second slice (K2.2) is similar, but derived with an additional intervening frame of either polarity. Thus, K2.1 measures neural recovery within the duration of one frame (16.7 ms with a 60 Hz frame rate), and K2.2 measures recovery over two frames (33 ms). On the basis of contrast gain, contrast saturation and peak latencies from VEP recordings at similar frame rates (Jackson et al. 2013; Klistorner et al. 1997), it was expected that the K2.1 response would be dominated by inputs of

magnocellular origin, while K2.2 would be dominated by parvocellular inputs.

## Analysis

Recorded data with associated stimulus hardware-generated triggers were initially pre-processed using MaxFilter (Elekta Neuromag) to project out sources of noise external to the spherical surface of the SQUID sensors. This also allowed for any bad channels to be rejected. In addition, the temporal signal space separation (tsss) routine (Taulu and Simola 2006) was used to minimize time-varying noise sources. The data were then imported into Brainstorm (Tadel et al. 2011) and epoched, and the kernel responses were calculated at the sensor level. Activations were projected onto the cortical surface via the MNE (minimum norm estimation) technique using the common brain Colin27 (<http://packages.bic.mni.mcgill.ca/tgz/>).

## Results

Following MaxFiltering (to remove projected noise sources), the epoched data were averaged around the triggers for onset and offset of the central stimulus patch. The waveforms of Fig. 1 show the outputs from the 204 planar gradiometer sensors. The difference in averages provided the first-order responses (K1—see Fig. 1a for a single participant). The second-order kernel slices were derived via a similar analysis with addition and subtraction of the averages of the four possible combinations of stimuli for the successive frames (K2.1—Fig. 1b and K2.2—Fig. 1c). See (Sutter 2000) for a simple description of the kernel extraction process.

Comparison of the low (24 %) and high (96 %) contrast mean amplitudes derived from an occipital cluster showed a marked amplitude growth with contrast for the major N60P90 peak in the first-order response (see Fig. 2). Also, at high contrast there is a “notch” in the waveform at a latency of approximately 65 ms, similar to that reported in K1 for the VEP (Sutherland and Crewther 2010). However, by comparison, the amplitude of the second-order first slice (K2.1) response was already saturated at the lower contrast (a similar reduction in amplitude of the K2.1 response is seen at high contrast in VEP (Klistorner et al. 1997)). The major peak of the second slice of the second-order kernel (K2.2) response (N90P110) showed twice the amplitude for high compared with low contrast. These findings are consistent with contrast response functions recorded with VEP (Jackson et al. 2013; Klistorner et al. 1997).

The process of estimating cortical activation was carried out with the MNE tools available within Brainstorm, using

the surface map of the common (Colin27) brain produced using Freesurfer (<https://surfer.nmr.mgh.harvard.edu>). The butterfly plot of average planar gradiometer activation across the five participants shows an excellent signal/noise ratio (Fig. 3a). The MNE-derived brain sources clearly demonstrate the expected pattern of activations, not only in calcarine occipital cortex, but also with discrete early cortical activations in the extrastriate cortex (see Fig. 3b). Five scout activations (average of MNE contributions from dipoles situated over a small group of mesh vertices on the cortical surface) located in occipital cortex were selected for further analysis. These are shown on the brain surface (Fig. 3b) and their location details (Talairach coordinates and nearest grey matter locations from Talairach Daemon: <http://www.talairach.org/client.html#CommandLine>) are to be found in Table 1. Activation in Right MT+ is highlighted in MRI viewer format in Fig. 3c.

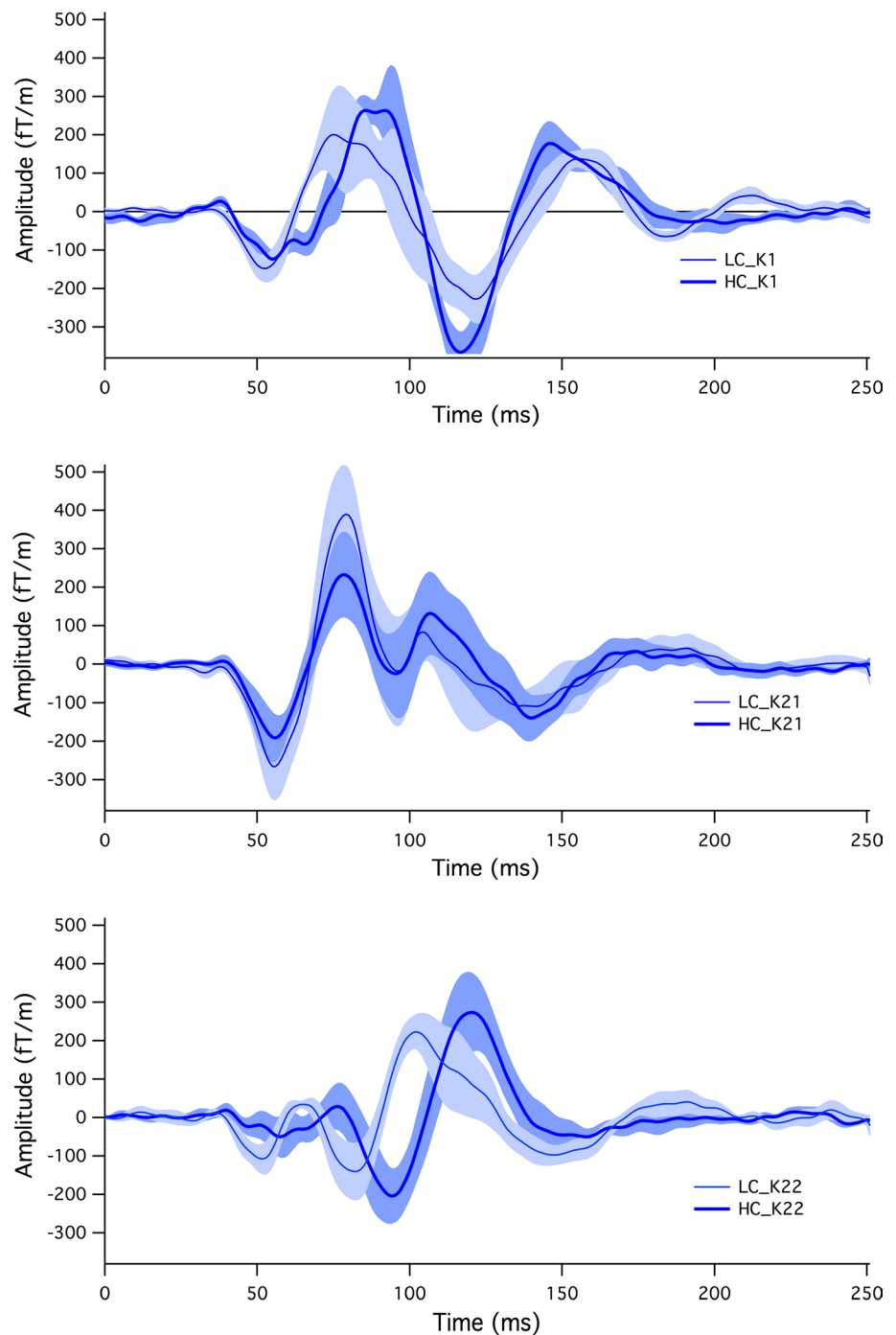
The question of which cortical regions are activated first was investigated through close comparison of individual and mean power generated by the V1 and MT+ scouts. The first order and first slice of the second-order evoked response power are shown for V1 and MT4 in Fig. 4 (the second slice shows greater latency and hence was not included in this analysis). Inspection of the four graphs shows that activation occurs in all regions well before 50 ms after stimulus onset. The pattern of K1 and K2.1 mean curves shows that the first-order power builds to reach a maximum at around 110 ms (Fig. 4a, b) while the K2.1 graphs show much more abrupt onset with peak power at around 80 ms (Fig. 4c, d). The regularity across participants is most apparent in the K2.1 response from MT+ (Fig. 4d), indicative of a transient, rapidly adapting neural source.

In order to answer the question of which response activation is most rapid, estimation was made, for each of the graphs in Fig. 4, of the mean and confidence interval of noise in the period (−50, 20 ms), prior to cortical activation. Estimation was then made of when the mean response curves first exceeded the upper 95 % confidence level of the noise. For the first-order K1 responses, initial activations were V1: 42 ms, MT+: 44 ms. For the second-order first slice K2.1 responses, initial activations were V1: 43 ms, MT+: 44 ms.

Time–frequency (TF) analyses of the five scout activations—from left occipital V1, left lingual gyrus (V2), left and right A19 and right MT+—were estimated for K1, K2.1 and K2.2 waveforms, using a Morlet wavelet transform available in Brainstorm (see Fig. 5). Here, a central frequency of 1 Hz and a time resolution of 1 s were chosen for the mother wavelet, with all other wavelets shifted and scaled variants of the mother wavelet.

The first-order TF responses from both scouts show maximum power for frequencies in the high alpha—low

**Fig. 2** Average cluster MEF (principal components derived) for low contrast (24 %—*thin line*) and high contrast (96 %—*thick line*) from a cluster of planar gradiometer sensors maximally activated over occipital cortex. The fringe around each mean curve represents  $\pm 1$ SE. The second slice of the second-order response (K2.2) shows evidence at low contrast of an early peak (N50P60) that is dominated by a longer latency wave for stimulation at high contrast



beta band, and with peak power occurring at around 100–110 ms. Some high-frequency (gamma band) activity is observable in all sites. The first slice K2.1 TF responses show much earlier activation for peak power (around 65 ms with frequency for peak power around 20 Hz in V1 and a little less in MT+). Gamma band activity is more prevalent and is prominent in V1, V2 and MT+ TF plots. The second slice K2.2 time–frequency plots show maximum power at 12–15 Hz, but

with longer latency for peak (105–110 ms) compared with the K2.1 TF responses.

## Discussion

This manuscript presents the first nonlinear analysis of MEG evoked fields and sources. The spatiotemporal analysis of results presented here with diffuse flashed stimuli is



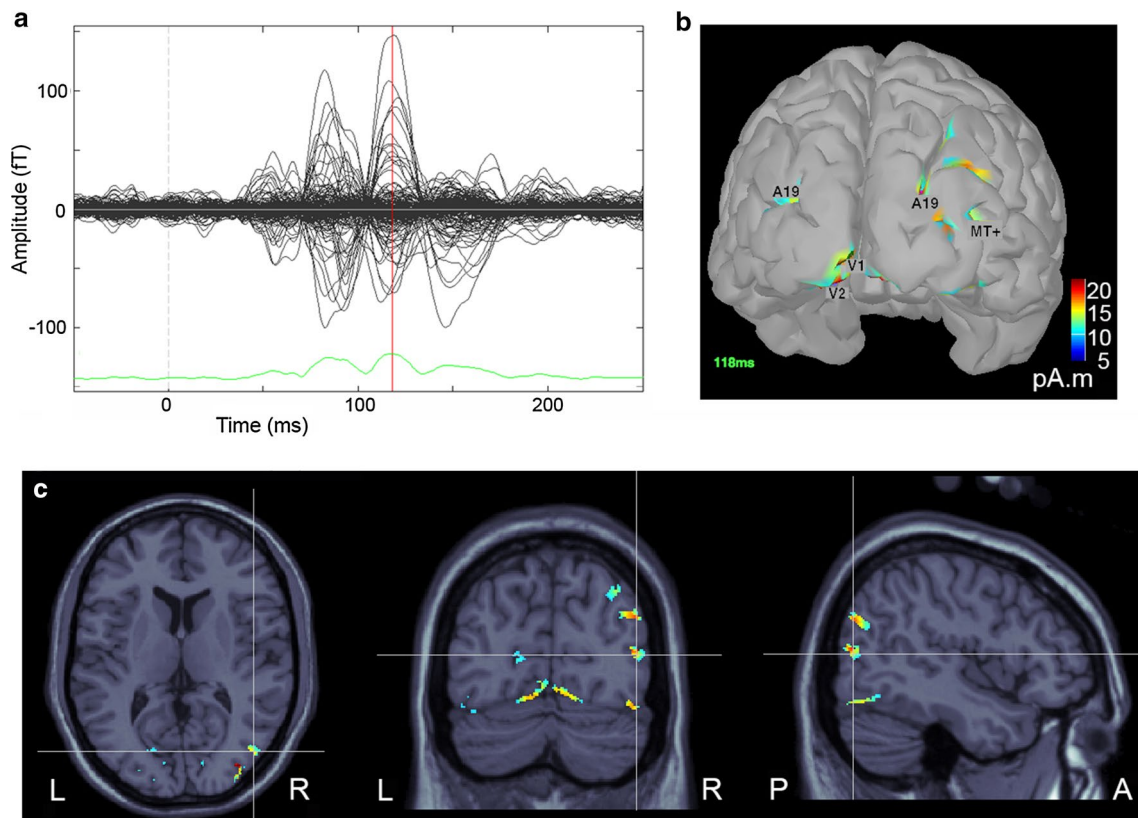


**Fig. 3** MNE source localization of first-order kernel response recorded at high contrast: **a** Average *butterfly plot* for the five participants, with showing an initial early activation peaking at around 55 ms and two later responses peaking at 80 and 118 ms (the *green line* represents the global field potential). **b** Minimum norm estimates

of first-order responses on the brain surface at 118 ms demonstrate the major occipital cortical regions activated. **c** 3D cortical image of MEG activation (K1, 118 ms) superposed onto the structural brain image. The *datum lines* shown intersect on MT+

**Table 1** Selected scout activation sites from MNE source localization

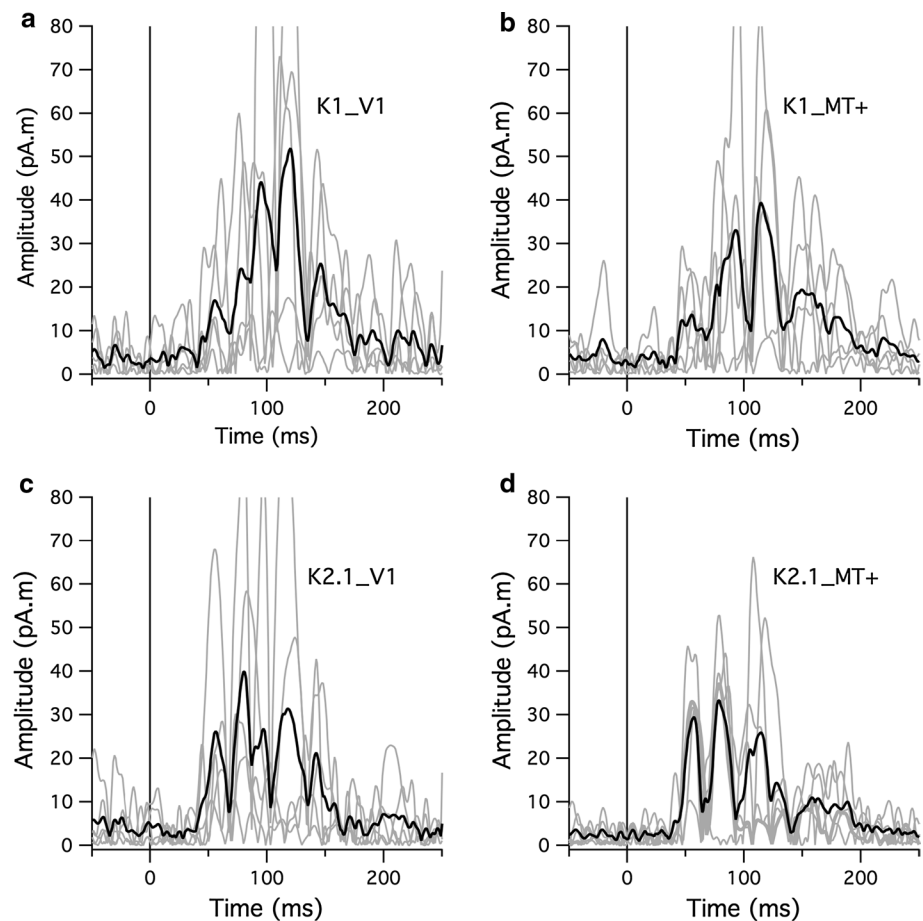
Scout name	$X_{TAL}$	$Y_{TAL}$	$Z_{TAL}$	
V1	-2	-92	-4	Left occipital, lingual gyrus, BA 17
V2	-9	-87	-18	Left occipital, lingual gyrus, BA18
A19_L	-26	-96	14	Left occipital, middle occipital gyrus, BA19
A19_R	28	-91	20	Right occipital, middle occipital gyrus, BA19
MT+	46	-73	8	Right occipital, middle occipital gyrus, BA 19

an extension of previous visual evoked potential multifocal studies (Jackson et al. 2013; Klistorner et al. 1997; Sutherland and Crewther 2010), demonstrating contrast responses and latency properties indicative of the ability to code magnocellular and parvocellular activity. In addition, the ability to localize sources on the cortical surface has opened up the question of the timing of initial cortical activation, previously only really studied in primates. Meta-analyses

of primate early visual processing demonstrate first neural spikes to activate V1 at around 35–40 ms with first spikes recordable from middle temporal area MT at around 40–42 ms (Bullier 2001; Lamme and Roelfsema 2000). The MNE source activations of Fig. 4 demonstrate that cortical activity in human is not far behind in timing compared with the early spike activity of monkey, with mean MEG activations becoming discernible above noise levels at around 42–44 ms for both areas V1 and MT+. These MEG latencies are in accordance with multifocal VEP recordings of around 43 ms (Jackson et al. 2013).

While conventionally it is thought that the major route to activation of V5/MT+ is through the LGN → V1 (4C $\alpha$ ) → V1 (layer IVB) → MT/V5 (Nassi and Callaway 2009), the results presented here might give cause for a rethink. Even if the time loss for each synapse is 2 ms (Maunsell et al. 1999), MT activation via this path should be delayed by at least 5–6 ms, compared with the earliest activation in V1. Instead, activation in MT/V5 is delayed by less than 2 ms compared with V1. Thus, it is possible that other inputs of the magnocellular ganglion cell output of the retina, e.g.

**Fig. 4** Individual time series of activation of the V1 and MT+ scout activations (derived from both magnetometers and gradiometers for the high-contrast stimulus condition) for the K1 and K2.1 responses. Also displayed in *heavier line* is the mean across the 5 participants' data. It is clear that the initial activation of the visual cortex occurs essentially simultaneously in these two sites. Note the rapid activation, consistent across participants, displayed in the K2.1 response from MT+



magno inputs via superior colliculus and pulvinar to MT+, could provide an alternative pathway, as recently demonstrated (Berman and Wurtz 2010).

Comparison of the first and second slices of the second-order responses from the five scout activations produces some interesting contrasts. Overall, differences in peak power must be discounted on the basis that the power recorded is dependent on the size of the mesh that is selected for each scout. However, as the K1, K2.1 and K2.1 TF plots were generated by the same recordings for each scout site, relative activity differences between the first- and second-order responses are worthy of report. The first such characteristic is the relative delay of K2.2 peak activity relative to that shown in K2.1. This is of the order of 30 ms, perhaps reflecting again the magnocellular advantage, given the fact that the overall contrast response of the first slice K2.1 response already appears saturated at a temporal contrast of 24 %. In addition, the K2.1 response showed higher-frequency contributions than K2.2 indicative of a neural drive more capable of high-frequency operation. One observation of interest is the fact that the K2.2 TF response for the V1 scout is relatively weak compared with first order, compared with the K2.2 versus K1 comparison for area V2 alongside. This could indicate that the

V1 neurons, particularly those driven by the parvocellular input, have relatively high neural efficiency, a feature that could derive from relatively weak stimulation of orientation selective simple cell receptive fields by diffuse patches of light.

The application of nonlinear analysis of MEG evoked signals to understanding the neuroscience of disorders of cognition is now a definite possibility. People with high autistic tendency show significantly larger second-order components driven by the magnocellular system (Jackson et al. 2013) and also abnormal high-contrast magnocellular function (Sutherland and Crewther 2010). In addition, early perceptual abnormalities in schizophrenia and autism have been addressed by other techniques involving nonlinear analysis (Butler et al. 2007; Lalor and Foxe 2009; Lalor et al. 2006; Sehatpour et al. 2010). However, to date, the ability to separate the responses from the different cortical areas for such transient signals with high temporal frequency content has been difficult.

The ability of MEG Wiener kernel analysis to clearly resolve V1 from MT+ and other extrastriate brain regions, as well as the ability to separate magnocellular from parvocellular contributions and the temporal priority of activation of different cortical regions, should prove increasingly

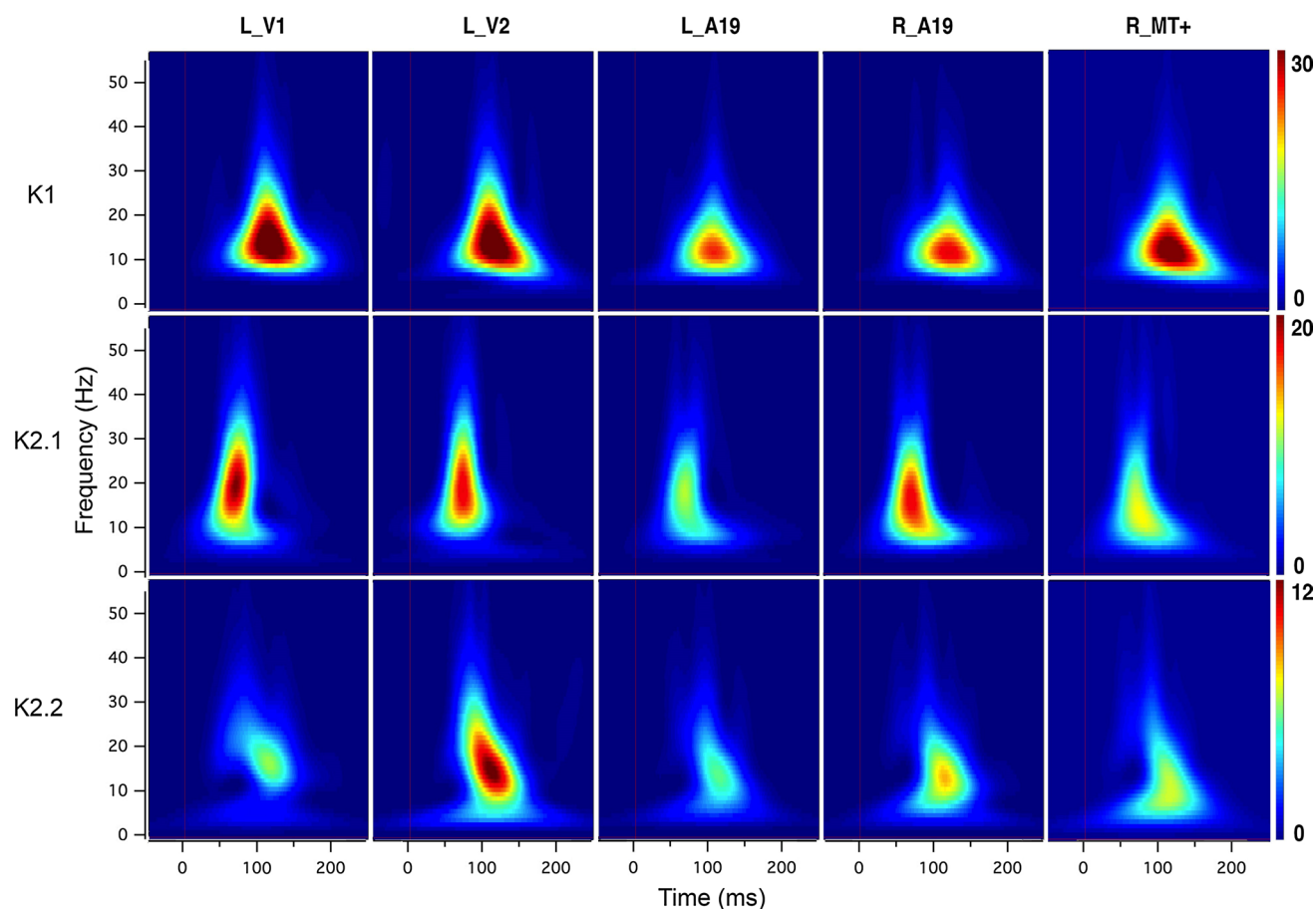


**Fig. 5** Time–frequency analysis of high-contrast (96 %) scout activations (Morlet transform of the average from the MNE-defined scouts of the five participants selected) of the first- and second-order (K1, K2.1 and K2.2) kernel responses from the five occipital cortical scouts. All second slice K2.2 responses show peak power that is delayed compared with first slice K2.1 by approximately 30 ms.

Relatively low K2.2 nonlinear intensity compared with K1 was observed in V1 compared with such comparison in V2. Colour bars represent a common scale across regions for K1, K2.1 and K2.2. The responses for each of the time–frequency maps have units of intensity of  $10^{-24}$  (pA.m)<sup>2</sup>

useful in the analysis of neurodevelopmental disorders of perception. It will provide clues as to the role that magnocellular activation plays in the early processes of perception, in particular, foreground/background segmentation and global versus local perception.

**Acknowledgments** The authors wish to acknowledge funding support of the National Health and Medical Research Council of Australia for project grant support (#1004740) and also the assistance of the staff of the Neuroimaging Facility at Swinburne University of Technology. The authors declare no competing financial interests.

## References

Baseler HA, Sutter EE, Klein SA, Carney T (1994) The topography of visual evoked response properties across the visual field. *Electroencephalogr Clin Neurophysiol* 90:65–81

- Berman RA, Wurtz RH (2010) Functional identification of a pulvinar path from superior colliculus to cortical area MT. *J Neurosci* 30:6342–6354. doi:10.1523/JNEUROSCI.6176-09.2010
- Bullier J (2001) Integrated model of visual processing. *Brain Res Brain Res Rev* 36:96–107
- Butler PD et al (2007) Subcortical visual dysfunction in schizophrenia drives secondary cortical impairments. *Brain* 130:417–430. doi:10.1093/brain/awl233
- Engel SA, Rumelhart DE, Wandell BA, Lee AT, Glover GH, Chichilnisky EJ, Shadlen MN (1994) fMRI of human visual cortex. *Nature* 369:525. doi:10.1038/369525a0
- Henriksson L, Karvonen J, Salminen-Vaparanta N, Railo H, Vanni S (2012) Retinotopic maps, spatial tuning, and locations of human visual areas in surface coordinates characterized with multifocal and blocked fMRI designs. *PLoS One* 7:e36859. doi:10.1371/journal.pone.0036859
- Hood DC, Greenstein VC (2003) Multifocal VEP and ganglion cell damage: applications and limitations for the study of glaucoma. *Prog Retin Eye Res* 22:201–251
- Hupe JM, James AC, Payne BR, Lomber SG, Girard P, Bullier J (1998) Cortical feedback improves discrimination between



- figure and background by V1, V2 and V3 neurons. *Nature* 394:784–787. doi:[10.1038/29537](https://doi.org/10.1038/29537)
- Hupe JM, James AC, Girard P, Lomber SG, Payne BR, Bullier J (2001) Feedback connections act on the early part of the responses in monkey visual cortex. *J Neurophysiol* 85:134–145
- Jackson BL et al (2013) Magno- and parvocellular contrast responses in varying degrees of autistic trait. *PLoS ONE* 8:e66797. doi:[10.1371/journal.pone.0066797](https://doi.org/10.1371/journal.pone.0066797)
- Kaplan E, Shapley RM (1986) The primate retina contains two types of ganglion cells, with high and low contrast sensitivity. *Proc Natl Acad Sci USA* 83:2755–2757
- Klistorner A, Crewther DP, Crewther SG (1997) Separate magnocellular and parvocellular contributions from temporal analysis of the multifocal VEP. *Vis Res* 37:2161–2169
- Lalor EC, Foxe JJ (2009) Visual evoked spread spectrum analysis (VESPA) responses to stimuli biased towards magnocellular and parvocellular pathways. *Vis Res* 49:127–133. doi:[10.1016/j.visres.2008.09.032](https://doi.org/10.1016/j.visres.2008.09.032)
- Lalor EC, Pearlmutter BA, Reilly RB, McDarby G, Foxe JJ (2006) The VESPA: a method for the rapid estimation of a visual evoked potential. *Neuroimage* 32:1549–1561. doi:[10.1016/j.neuroimage.2006.05.054](https://doi.org/10.1016/j.neuroimage.2006.05.054)
- Lamme VA, Roelfsema PR (2000) The distinct modes of vision offered by feedforward and recurrent processing. *Trends Neurosci* 23:571–579
- Laycock R, Crewther SG, Crewther DP (2007) A role for the ‘magnocellular advantage’ in visual impairments in neurodevelopmental and psychiatric disorders. *Neurosci Biobehav Rev* 31:363–376. doi:[10.1016/j.neubiorev.2006.10.003](https://doi.org/10.1016/j.neubiorev.2006.10.003)
- Laycock R, Crewther DP, Crewther SG (2008) The advantage in being magnocellular: a few more remarks on attention and the magnocellular system. *Neurosci Biobehav Rev* 32:1409–1415. doi:[10.1016/j.neubiorev.2008.04.008](https://doi.org/10.1016/j.neubiorev.2008.04.008)
- Maunsell JH, Ghose GM, Assad JA, McAdams CJ, Boudreau CE, Noerager BD (1999) Visual response latencies of magnocellular and parvocellular LGN neurons in macaque monkeys. *Vis Neurosci* 16:1–14
- Nassi JJ, Callaway EM (2009) Parallel processing strategies of the primate visual system. *Nat Rev Neurosci* 10:360–372
- Nishiyama T, Ohde H, Haruta Y, Mashima Y, Oguchi Y (2004) Multifocal magnetoencephalogram applied to objective visual field analysis. *Jpn J Ophthalmol* 48:115–122. doi:[10.1007/s10384-003-0044-9](https://doi.org/10.1007/s10384-003-0044-9)
- Sehatpour P, Dias EC, Butler PD, Revheim N, Guilfoyle DN, Foxe JJ, Javitt DC (2010) Impaired visual object processing across an occipital-frontal-hippocampal brain network in schizophrenia: an integrated neuroimaging study. *Arch Gen Psychiatry* 67:772–782. doi:[10.1001/archgenpsychiatry.2010.85](https://doi.org/10.1001/archgenpsychiatry.2010.85)
- Sereno MI et al (1995) Borders of multiple visual areas in humans revealed by functional magnetic resonance imaging. *Science* 268:889–893
- Super H, Lamme VA (2007a) Altered figure-ground perception in monkeys with an extra-striate lesion. *Neuropsychologia* 45:3329–3334. doi:[10.1016/j.neuropsychologia.2007.07.001](https://doi.org/10.1016/j.neuropsychologia.2007.07.001)
- Super H, Lamme VA (2007b) Strength of figure-ground activity in monkey primary visual cortex predicts saccadic reaction time in a delayed detection task. *Cereb Cortex* 17:1468–1475. doi:[10.1093/cercor/bhl058](https://doi.org/10.1093/cercor/bhl058)
- Sutherland A, Crewther DP (2010) Magnocellular visual evoked potential delay with high autism spectrum quotient yields a neural mechanism for altered perception. *Brain* 133:2089–2097. doi:[10.1093/brain/awq122](https://doi.org/10.1093/brain/awq122)
- Sutter EE (1992) A deterministic approach to nonlinear systems analysis. In: Pinter RB, Nabet B (eds) *Nonlinear vision*. CRC Press, Cleveland, pp 171–220
- Sutter E (2000) The interpretation of multifocal binary kernels. *Doc Ophthalmol* 100:49–75
- Tabuchi H, Yokoyama T, Shimogawara M, Shiraki K, Nagasaka E, Miki T (2002) Study of the visual evoked magnetic field with the m-sequence technique. *Investig Ophthalmol Vis Sci* 43:2045–2054
- Tadel F, Baillet S, Mosher JC, Pantazis D, Leahy RM (2011) Brainstorm: a user-friendly application for MEG/EEG analysis. *Comput Intell Neurosci* 2011:879716. doi:[10.1155/2011/879716](https://doi.org/10.1155/2011/879716)
- Taulu S, Simola J (2006) Spatiotemporal signal space separation method for rejecting nearby interference in MEG measurements. *Phys Med Biol* 51:1759–1768. doi:[10.1088/0031-9155/51/7/008](https://doi.org/10.1088/0031-9155/51/7/008)
- Vanni S, Henriksson L, James AC (2005) Multifocal fMRI mapping of visual cortical areas. *NeuroImage* 27:95–105. doi:[10.1016/j.neuroimage.2005.01.046](https://doi.org/10.1016/j.neuroimage.2005.01.046)